LLNL-JRNL-812492

LAWRENCE
LIVERMORE
NATIONAL
LABORATORY

Analysis of defects in In2O3:H synthesized in presence of water vapor and hydrogen gas mixture

A. Samanta, J. Varley, V. Lordi

July 15, 2020

Journal of Applied Physics

Disclaimer

Analysis of defects in In_2O_3:H synthesized in presence of water vapor and hydrogen gas mixture

Amit Samanta*
Physics Division, Lawrence Livermore National Laboratory, Livermore, California 94550, USA

Joel Varley and Vincenzo Lordi
Materials Science Division, Lawrence Livermore National Laboratory, Livermore, California 94550, USA

(Dated: December 19, 2020)

Using hybrid functional-based density functional theory calculations, we analyze the structure and kinetics of defects formed in two competing synthesis routes to prepare hydrogen-doped In_2O_3 films: using a hydrogen and oxygen gas mixture vs synthesis in presence of water vapor. For both of these two synthesis routes, we find that H^+ is the dominant defect species: when the Fermi level is close to the conduction band, H^+ has a lower formation energy than other intrinsic or extrinsic defects. Our results also suggest that water molecules spontaneously split into H^+ (which occupies octahedral voids) and OH^- interstitials (which occupies vacant oxygen lattice sites or oxygen vacancies). From the analysis of the binding energies between these different defects, we conclude that these defects do not cluster and are most likely to stay spatially distributed throughout the films. In addition, the sum of formation energies of an oxygen (i.e. O_i^{2-}) and a H^+ interstitial are close to the formation energy of a OH^- interstitial meaning that water molecules are completely split into $2H^+$ and O_i^{2-}, at the synthesis conditions. Further, in the presence of H_2 + O_2 gas mixture, oxygen interstitials occupy oxygen vacancies while hydrogen interstitials occupy vacant oxygen lattice sites and form bonds with lattice oxygens. Our analysis of the defect equilibria suggests that hydrogen content in films synthesized in the presence of water vapor is higher than films synthesized in the presence of a hydrogen gas mixture. At high dopant concentrations, a hydrogen bond network is formed in the system and this leads to large distortions in the lattice.

I. INTRODUCTION

Hydrogen-doped indium oxide (In_2O_3:H) is a promising material for solar cell and photo detector applications and can potentially replace commercially used In_2O_3:Sn. This interest in In_2O_3:H originated with a series of papers published by Koida, Fujiwara and Kondo in 2007-2010 in which they demonstrated that In_2O_3 films (of 70-240 nm thickness) prepared by using a radio frequency magnetron sputtering system in presence of oxygen and water vapor, followed by annealing at 200 °C for 2 hours, exhibited high mobility (98-140 cm^2/Vs) and high near-infrared transparency (more than 94 %).[1–3] For comparison, we note that typical values of Hall mobility for In_2O_3:Sn (10%) are $20-40$ cm^2Vs (carrier concentration $\sim 10^{21}$$cm^3$, resistivity $\sim 5 \times 10^{-4}$ Ωcm).[4–6] In Ref. [1], it is reported that with an increase in the partial pressure of water vapor from 5×10^{-6} Pa to 5×10^{-3} Pa, the concentration of hydrogen in the films increases from 0.35 to 8.8 at. %. Thus, it is intuitive to ask where all these hydrogens are residing in In_2O_3 and whether some of these hydrogens can also exist as H_2 molecules?

In addition, the analysis of thermal desorption spectra of gases exiting the In_2O_3:H samples upon heating to 650 °C suggests that water vapor decomposes to H^+ and OH^- during the sputter deposition process and these species form bonds with In and O present in the growing surface during synthesis.[3] From their analysis, Koida et al. concluded that sputtering in the presence of oxygen and water vapor followed by an annealing treatment eliminates oxygen deficiency and generates H^+ singly charged donors meaning that charge carriers are H^+ and not oxygen vacancies.[3] In fact, by using X-ray photoluminescence spectroscopy and Rutherford backscattering spectroscopy, Macco et al. have shown that the ratio of oxygens to indiums in In_2O_3 is ∼1.58, higher than the ratio of 1.50 for the ideal structure.[7] It is possible that the oxygen gas used during the synthesis is the source of this extra oxygen, which can reside as oxygen interstitials in In_2O_3. Interestingly, Jost et al. have reported that the electrical and optical properties of films are not very sensitive to small changes in oxygen fraction used during synthesis.[8] Thus, it is clear that a better understanding of the role played by the O_2 gas that enters the sputtering chamber (along with water vapor) and the relationship between the concentration of defects, like H^+, to the partial pressure of water vapor or oxygen gas can help in further optimizing the synthesis conditions. In addition, by using heavy water during the synthesis of In_2O_3:H, Wu et al. have reported that the hydrogen in In_2O_3 is homogeneously distributed in the bulk of the material.[9] Does this mean that, unlike In_2O_3:Sn, complicated defect complexes are not formed in In_2O_3:H?

First principles calculations suggest that both H^+ in antibonding sites and hydrogen in a vacant oxygen site have low formation energies and are shallow donors.[10,11] There is experimental evidence to support this result: analysis of paramagnetic charge state of muonium by King et al. also points to the presence of shallow donors.[12,13] Anionic defects in In_2O_3 have been extensively studied using first principles calculations,[14–18] but their role is probably limited in In_2O_3:H because local density approximation, LDA, based DFT calculations performed by Limpijumnong et al. show that when the Fermi level is below $\mu_e = 0.60$ eV, V_O^{2+} has a lower formation energy than H^+. On the other hand, when the Fermi level is close to the conduction band, H^+ has a lower formation energy.[10] Therefore, it is important to verify this result using a more accurate level of calculation and for different environmental conditions.

In 2016, Jost and co-workers[8] proposed an alternate route to prepare hydrogen-doped In_2O_3 by using a mixture of H_2

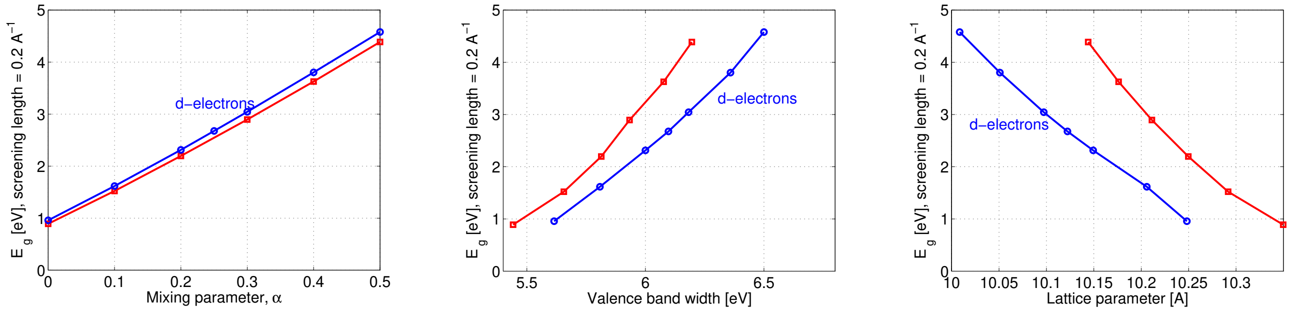

(a) (b) (c)

FIG. 1: Shown here are the variations in band-gap ($E_{\rm g}$), lattice parameter, and valence band width ($\Delta_{\rm VB}$) of In_2O_3 for two different pseduo-potentials of indium (with and without d-electrons) and different values of the exact exchange mixing parameter (α).

and O_2 gases during the sputtering process instead of using a mixture of water vapor and oxygen gas as used by Koida et al,[1] or by Libera et al.[19] In addition, it has been shown that the variation in optical and electrical properties of multiple films deposited using a hydrogen gas mixture are much lower than films prepared by using the water vapor route.[8] This is attributed to the fact that synthesis in the presence of water vapor introduces uncertainties in the quantity of water vapor entering the sputtering chamber and on the properties of the films. Since the electrical and optical properties of films deposited in presence of hydrogen gas mixture are close to those of films synthesized using water vapor, a first principles analysis of the defects formed during these two competing synthesis routes can help in optimizing the synthesis procedure. This becomes important because Boccard et al. have recently reported that simply introducing H_2 gas into the chamber results in an increase in the mobility of In_2O_3 from 40-60 cm^2/Vs for undoped films to 80 cm^2/Vs for films deposited in presence of hydrogen.[20]

Even though Hall mobilities and optical transparencies of films prepared using both of these techniques are similar, Jost et al. have found that the overall concentration of hydrogen in samples prepared using the hydrogen gas mixture route is lower than those in films deposited in presence of water vapor.[8] This decrease in hydrogen concentration can be attributed to a potentially different mechanism of incorporation of hydrogen in the films (compared to films synthesized using water vapor) or passivation of defects at grain boundaries by hydrogens.[8] Thus, it is important to understand how hydrogen is incorporated into the films and the relationship between partial pressure of the hydrogen gas and the concentration of H^+ defects.

The high mobility ($>$100 cm^2/Vs) of In_2O_3:H at a carrier concentration of $\sim$10^{20} cm^{-3} and high transparency has generated a lot of excitement among researchers.[2,21] For example, silicon hetero-junction solar cells containing In_2O_3:H films exhibit higher short-circuit current densities than Sn-doped indium oxide films.[22] Similarly, carrier mobilities reported for In_2O_3:H in Cu(In, Ga)Se solar cells are much higher than currently used ZnO:Al films.[23] Apart from applications in solar cells, In_2O_3 has also been studied for applications such as sensors for hydrogen gas. For example, Zheng et al. have reported that one dimensional In_2O_3 nanostructures have very good hydrogen gas sensing capabilities for a hydrogen concentration of 2$-$1000 parts per million at 120-275 °C.[24] The hydrogen gas sensing capability of In_2O_3 nanostructures is attributed to the decrease in resistivity due to the abundance of oxygen vacancies. Thus, an analysis of how H_2 interacts with In_2O_3 can potentially lead to the design of better sensors.

It is clear from the discussion presented above that a systematic first principles analysis of how the hydrogen gas mixture interacts with In_2O_3 can help to clarify many unresolved issues. Thus, in this contribution, using hybrid functional based density functional theory calculations we analyze how hydrogen molecules interact with In_2O_3, identify the dominant defect species and study its thermodynamic stability at finite temperature and pressure conditions. In addition, we analyze if the dominant defect changes when a large concentration of hydrogen molecules are incorporated into In_2O_3. To understand how the films deposited in presence of hydrogen and water vapor differ, we also analyze the structure and kinetics of defects formed when one, two or many water molecules are simultaneously incorporated into In_2O_3.

II. COMPUTATIONAL DETAILS

To analyze the electronic structure, we perform HSE (Heyd-Scuseria-Ernzerhof)[25] hybrid functional calculations using the plane wave basis density functional theory (DFT) with projected augmented wave method (PAW) implementation in Vienna Ab-initio Simulation Package (VASP).[26,27] We use 560 eV as the plane wave cutoff to expand the wavefunctions and 2×2×2 **k**-point mesh for integrations in the first Brillouin zone. For all electronic structure and defect stability analysis, we use the conventional 80 atoms unit cell containing 16 formula units of In_2O_3. To account for the periodic image interactions in supercells containing charged defects, we use the Makov-Payne based scheme to correct the total energies obtained from DFT calculations.[28] For the hy-

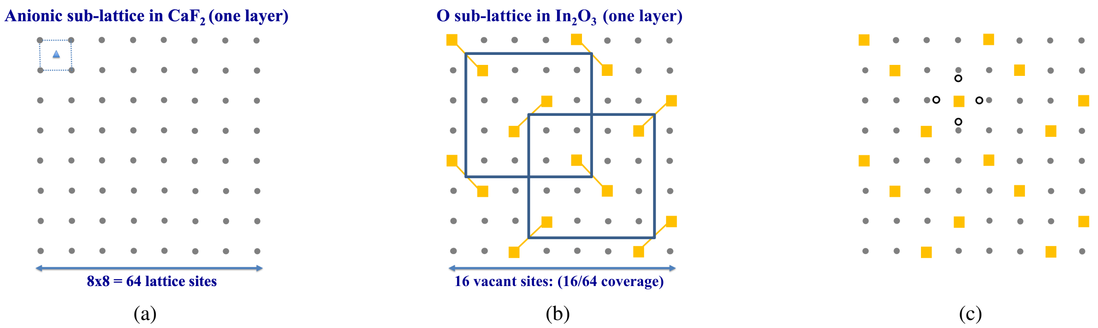

FIG. 2: Schematic representations of the arrangements anions on a single (001) plane of CaF_2 ($2(a)$) and In_2O_3 ($2(b)$ and $2(c)$). Solid circles, square markers and open circles denote anionic/oxygen sites, vacant oxygen lattice sites and hydrogen interstitial sites, respectively. The solid lines in $2(b)$ highlight the ordering of the vacant oxygen lattice sites. As shown in $2(a)$ the octahedral voids (marked with a triangle) are located out of the plane, at the enter of the square with four oxygens at the corners.

brid functional calculations, the screening parameter is set to $\mu = 0.20$ Å and the change in the band-gap as a function of the mixing parameter, α, is shown in Fig. $1(a)$.

We use tested different pseudo-potentials for indium: one with 3 valence electrons (i.e. $5s$ and $5p$ states) and another with 13 valence electrons (i.e. $5s$, $5p$ and $4d$ states). This is motivated by the strong coupling between In $4d$ and O $3p$ states reported by King et al. in Ref. [29]. Since, the inclusion of the d-electrons in the calculations affects the lattice parameter as well as the valence band width (see Figs. $1(c)$ and $1(b)$, respectively), we use the pseudo-potential with 13 valence elements for all subsequent analyses presented here.

The width of the valence band, Δ_{VB}, has been suggested to be a good measure of the cohesive interaction between atoms in a system, and that by using an accurate value of the valence band width (from a higher level of theory), it is possible to reliably estimate the fraction of exact exchange required to correctly reproduce the band gap and defect formation energies.[30] We use the experimental value of the valence band width, i.e. $\Delta_{\mathrm{VB}} \approx 6.15$ eV, measured by King et al. from the photoemission spectrum after accounting for lifetime and instrumental broadening effects.[29] Thus, from Fig. $1(b)$ we see that $E_{\mathrm{g}}{\sim}3.5$ eV when $\Delta_{\mathrm{VB}}{\sim}6.15$ eV (see Ref. [29]). But, recent experimental predictions of the band-gap of In_2O_3 lie in the range of 2.90-2.93 eV.[29,31–33] Thus, we use a mixing parameter of $\alpha = 0.282$ which leads to a band-gap of $E_{\mathrm{g}} = 2.91$ eV and a lattice parameter of 10.182 Å.

To calculate the defect formation free energies at a given temperature and pressure, we calculate the free energies of supercells containing defects by including their vibrational free energies. We calculate the Helmholtz free energies of different systems by including the vibrational free energy contributions within the harmonic approximation. For example, the free energy of bulk indium oxide, $F\left(\mathrm{In_2O_3}\right)$, is given by $F\left(\mathrm{In_2O_3}\right) = E\left(\mathrm{In_2O_3}\right) + F_{\mathrm{vib}}\left(\mathrm{In_2O_3}\right)$. Here, $E\left(\mathrm{In_2O_3}\right)$ is the energy of an indium oxide bulk supercell,

$$F_{\mathrm{vib}}\left(\mathrm{In_2O_3}\right) = k_B T \sum_q \left\{ \frac{\hbar\omega_q}{2k_B T} + \ln\left[1 - e^{-\hbar\omega_q/k_B T}\right] \right\} \tag{1}$$

is the vibration free energy contribution within the harmonic approximation, $\hbar$ is the reduced Plank constant, ω_q ($q = 1, 2, \ldots$ n_{DOF}) are the vibration frequencies and n_{DOF} is the number of degrees of freedom in the system after excluding the global rotation and translation degrees of freedom. For the range of pressures considered in our analysis, changes in volumes of supercells used in our calculations are very small. Thus, the effect of pressure on the phonon frequencies are neglected. We use a similar procedure to calculate the formation free energies of defects and defect complexes involving intrinsic defects, hydrogen and water molecules. To study the thermodynamic stability of defects, the chemical potentials for hydrogen, oxygen and water molecules are calculated using the procedure outlined in Ref. [34–36].

To understand the kinetics of defects, and in order to verify the ground state defect configurations, we also perform high temperature molecular dynamics (MD) simulations using supercells containing 80 (the conventional cubic unit cell) and 640 atoms (2×2×2 of the conventional cubic unit cell). Since hybrid functional calculations are computationally expensive, we use the PBE (Perdew-Burke-Ernzerhof) functional[37] for these calculations and evolved the systems at 1000, 1500 and 2000 K for about ∼8-10 pico-seconds. Due to the short timescales accessible in DFT calculations, such high temperatures allow us to accelerate kinetics of the physical processes. For these calculations, we use a 2×2×2 (for the 80 atoms supercell) or a 1×1×1 (for the 640 atoms supercell) **k**-points grid for Brillouin zone integration.

III. RESULTS

A. Hydrogen molecules in In_2O_3

One hydrogen interstitial: Figure 2 compares the arrangement of anionic lattice sites in CaF_2 and In_2O_3, and Fig. 2(c) shows the probable sites where hydrogens can be introduced into In_2O_3. In a neutral supercell, our results show that the ground state geometry of a hydrogen interstitial corresponds to an interstitial in a vacant oxygen lattice site of In_2O_3 and it is not bonded to any neighboring oxygens of the In_2O_3 lattice.A defect state corresponding to this interstitial is located ~1.3 eV above the valence band maximum. In the ground state structure, a H^+ interstitial forms a bond (bond length is 0.98 Å) with an oxygen of In_2O_3 and the next nearest oxygen of the lattice atom is ~1.76 Å away from the interstitial.

Figure 3 shows the formation free energies of hydrogen interstitials at 0 K and at 500 K which is close to the annealing temperature used during synthesis of In_2O_3:H films. The interstitial formation free energy is given by

$$F_{\rm f}\left(\mathrm{H_i^+}\right) = F\left(\mathrm{In_2O_3} + \mathrm{H_i^+}\right) - \mu_{\rm H} + \mu_e - F_{\rm bulk} + \Delta, \quad (2)$$

where, $\mu_{\rm e}$ is the chemical potential (Fermi energy) of electrons, $\mu_{\rm H}$ is the chemical potential of hydrogen at a given temperature and partial pressure of H_2 gas, $F_{\rm bulk}$ is the free energy of the bulk defect-free supercell, $F\left(\mathrm{In_2O_3} + \mathrm{H_i^+}\right)$ is the free energy of a supercell containing a vacant lattice site and net charge of +e, and Δ is the correction to appropriately align the electrostatic potential of a bulk supercell with the electrostatic potential in the bulk like region of a supercell containing a defect. The chemical potential of hydrogen, $\mu_{\rm H}$, is taken to be half of the free energy of a hydrogen molecule (calculated using the ideal gas approximation) in a large supercell.[34] Here we note that Eq. 2 is modeled according to the following reaction

$$\frac{1}{2}\mathrm{H_2}\,(\mathrm{gas}) \Longleftrightarrow \mathrm{H^+} + \mathrm{e^-} \quad (3)$$

meaning that the atmosphere is taken to be the source of hydrogens entering In_2O_3. It is clear from Fig. 3(a) that the charge transition level $(+/-)$ lies in the conduction band.

Two hydrogen interstitials: In a neutral supercell, in the ground state configuration, a hydrogen molecule occupies a vacant oxygen lattice site (see Fig. 4(a)). The H−H bond length is 0.74 Å and the nearest oxygen is 1.97 Å away from the H_2 molecule.

In a doubly charged supercell (i.e. two electrons are removed from a neutral supercell containing two hydrogen interstitials), the H_2 molecule is split into two H^+ interstitials. In the ground state configuration, both of these interstitials form bonds with lattice oxygens and the separation between interstitials is 4.07 Å. In addition, these interstitials also form a hydrogen bond network: the O−H bond lengths are 0.98 Å and distances between the interstitials and their next nearest neighbor oxygens are 2.02-2.04 Å. Figure 5(a) shows the formation energies of a hydrogen molecule and two H^+ interstitials. Clearly, a H^+ interstitial has lower a formation energy and when the Fermi level is close to the conduction band minimum both these defects have similar formation energies.

In a singly charge supercell (i.e. when an electron is removed from the supercell containing two hydrogen interstitials), one hydrogen interstitial occupies a vacant oxygen lattice site while the other hydrogen interstitial forms a O−H bond (bond length is 0.98 Å) with an oxygen of the lattice.

Four, six and eight hydrogen interstitials: We explored many different configurations for a system containing two, three and four hydrogen molecules. In the ground state, two or more hydrogen molecules also split into H^+ interstitials. These interstitials form bonds with oxygens of the lattice and are located close to vacant oxygen lattice sites as shown in Fig. 2(c). In addition, these interstitials are organized in a way that the O−H bond length is ~0.97 Å and the second nearest oxygen of the lattice is about ~1.86 Å away from the H^+ interstitial. Thus, for all the H^+ interstitials, the second nearest oxygens are shifted from their respective lattice sites by 0.70 Å, and this introduces a distortion in the oxygen sublattice of In_2O_3. Figures 5(b) and 5(c) show the formation energies of interstitials in different charge states.[38]

Figure 5(d) shows that the formation energies of hydrogen interstitials in a neutral supercell increases monotonically with an increase in the number of water molecules. Using a linear fit, the formation energy is given by $E_{\rm f}\left(n_{\rm H_2}\mathrm{H_2}\right) = 4.88 n_{\rm H_2} - 0.87$ eV. Here, $n_{\rm H_2}$ is the number of hydrogen molecules in the system. Thus, the binding energy between the different hydrogen molecules is about ~0.87 eV meaning that hydrogen molecules do not form clusters.

B. Intrinsic defects

Figure 3(a) shows the formation energy of oxygen interstitials (placed at vacant oxygen lattice sites) and vacancies in undoped In_2O_3 at 0 K. The vacancy formation free energy is given by

$$F_{\rm f}\left(\mathrm{V_O^{q+}}\right) = F\left(\mathrm{In_2O_3} + \mathrm{V_O^{q+}}\right) + \mu_{\rm O} + q\mu_e - F_{\rm bulk} + \Delta, \quad (4)$$

where, $\mu_{\rm O}$ is the chemical potential of oxygen, $F\left(\mathrm{In_2O_3} + \mathrm{V_O^{q+}}\right)$ is the free energy of a supercell containing a vacant lattice site and net charge of +2e. $\mu_{\rm O}$ is taken to be half of the energy of an oxygen molecule in a large supercell. Here we note that Eq. 4 physically represents the following reaction

$$\mathrm{O_O} \Longleftrightarrow \frac{1}{2}\mathrm{O_2}\,(\mathrm{gas}) + \mathrm{V_O^{2+}} + 2e^- \quad (5)$$

and, hence, the reference state of oxygen is an oxygen gas molecule, i.e. the atmosphere is the sink/reservoir for oxygens leaving In_2O_3.

Figure 3 also shows the dependence of the formation free energy of anionic defects (in undoped In_2O_3) on the oxygen partial pressure ($p_{\rm O_2}$). If we consider only isolated intrinsic anionic defects, we see that the Fermi level is pinned at $\mu_{\rm e}$~2.30 eV at 0 K. But, with an increase in temperature, this level shifts to 2.40 eV at 400 K and 1 atm, and to 2.60 eV

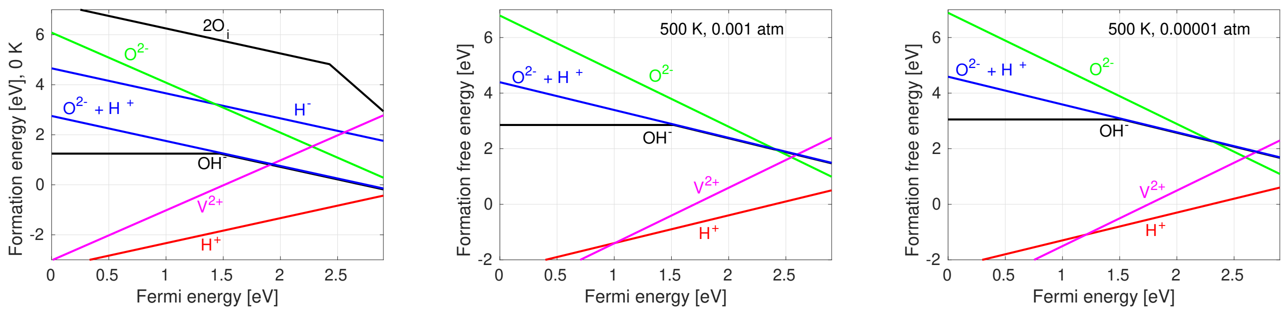

(a) (b) (c)

FIG. 3: Analysis of formation energies of oxygen vacancies and interstitials, hydrogen and OH interstitials in undoped In_2O_3 at different temperature and oxygen partial pressure conditions are shown in $3(a) - 3(c)$. The reference states for oxygen, hydrogen and water were taken to be a oxygen, hydrogen or water molecule in a large simulation box.

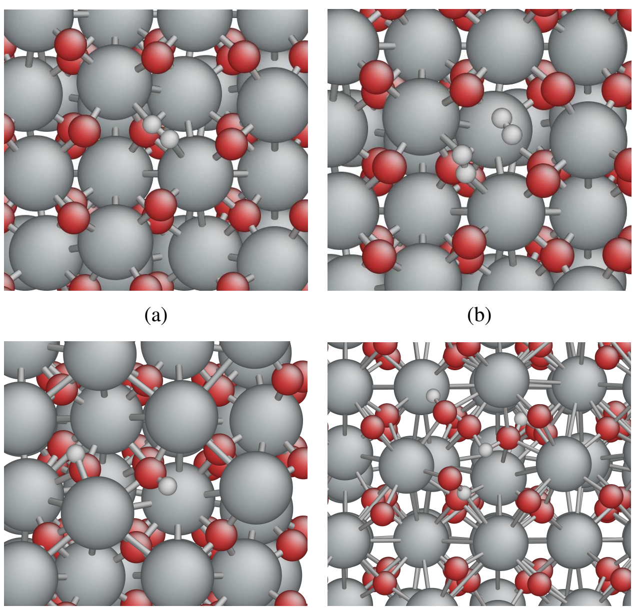

(a) (b) (c) (d)

FIG. 4: The ground state configurations of neutral supercells containing one H_2 molecule, and two H_2 molecules are shown in $4(a)$, $4(b)$, respectively. $4(c)$ and $4(d)$ show the ground state configuration of one and two water molecules, respectively.

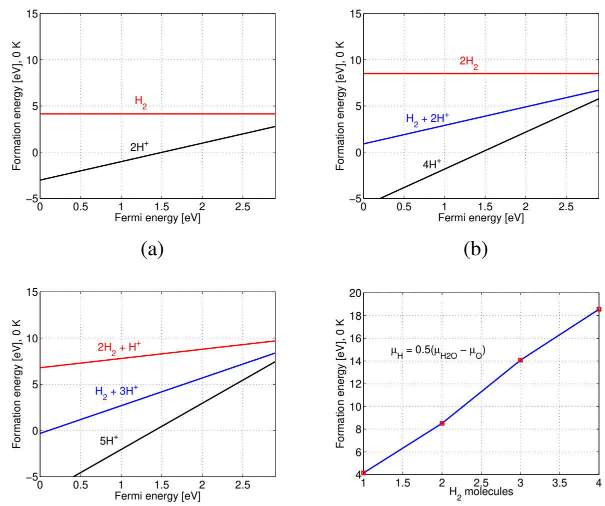

(a) (b) (c) (d)

FIG. 5: Shown here are the formation energies of hydrogen interstitials in their different charge states in supercells containing different number of hydrogen interstitials.

at 400 K and 10^{-10} atm (i.e. at very low pressures, close to ultr-high vacuum conditions - these conditions represent the extremes of the range of possibilities). Similarly, when the temperature is set to 500 K, the Fermi level is pinned at $\mu_e \sim 2.5$ and ~ 2.7 eV at 1 and 10^{-10} atm, respectively.

Figure $3(a)$ also compares the formation energies of a system containing two oxygen interstitials with a system containing a single oxygen interstitial.[39] When the Fermi level is close to the conduction band minimum, we see that $E_f\,(2O_i) \approx 2E_f\,(O_i)$ (valid only for formation energies without periodic image interaction corrections). This means that binding energy between oxygen interstitials is close to zero, and these interstitials do not exhibit any tendency to form clusters.

C. Water molecules in In_2O_3

To understand how water molecules interact with In_2O_3, we incorporate up to eight water molecules in the conventional 80 atoms unit cell of In_2O_3. These dopants correspond to 2.46 to 15.40 at.% of hydrogens in the system, respectively. Our results show that water molecules spontaneously split into H^+ and OH^- interstitials. As shown in Fig. $4(c)$, the OH^- interstitial occupies a vacant oxygen lattice site, and the H^+ interstitial occupies an octahedral void and forms a bond with a lattice oxygen (0.97 Å bond length). This lattice oxygen is displaced from its original lattice site by about 0.70 Å. In addition, the second nearest lattice oxygen is 1.85 Å away from the interstitial. A similar splitting is evident when more than one water molecules are incorporated into a supercell containing 80 atoms and a considerable distortion of the oxygen sub-lattice is also observed. This increase in distortion of the oxygen sub-lattice with increase in dopant concentration is also evident from projections of positions of oxygens (see Fig. 6) in configurations obtained from high temperature MD simulations (at 1000 K). The displaced oxygens (marked with $\mathrm{O_d}$ in Fig. 6) are attached to hydrogen interstitials located in octahedral voids. The projection of positions of oxygens (on the two-dimensional yz-plane, see Fig. $6(b)$) in the supercell with eight water molecules also suggests that at higher dopant concentrations this distortion enhances the migration of oxygens.

We find the formation energies of incorporating water molecules in $\mathrm{In_2O_3}$ vary linearly with the number of water molecules, i.e. $E_\mathrm{f}\left(n_{\mathrm{H_2O}}\mathrm{H_2O}\right) = 1.86 n_{\mathrm{H_2O}} - 0.037$ eV, where $n_{\mathrm{H_2O}}$ is the number of water molecules in the system.[11] The reference state for the formation energy analysis is a water molecule in a large simulation box. Such a linear relationship shows that in a typical water doped indium oxide sample, water molecules do not like to form clusters (binding energy $\sim$0.037 eV), or in other words, the $\mathrm{H^+}$ and $\mathrm{OH^-}$ interstitials are spatially separated and diffuse easily. To further verify this hypothesis, we perform high temperature MD simulations and analyze the intermediate configurations.

Stability of an isolated OH interstitial: Since water molecules split into $\mathrm{H^+}$ and $\mathrm{OH^-}$ defects, we also analyze the stability of an isolated OH interstitial. We see that a negatively charged OH interstitial at an octahedral site has only 0.07 eV lower energy than an interstitial in a vacant oxygen lattice site. Given this small energy difference between these two $\mathrm{OH^-}$ configurations it is possible that after a water molecule splits, the $\mathrm{OH^-}$ interstitial can occupy either of these configurations. We see a similar splitting of a water molecule when it is placed at an oxygen vacancy. In fact, the $\mathrm{OH^-}$ interstitial occupies the vacancy and the $\mathrm{H^+}$ interstitial forms a bond with an oxygen of $\mathrm{In_2O_3}$.

As shown in Fig. $4(d)$, configurations containing two or more water molecules also exhibit a similar pattern of splitting. To explore the different possible configurations and to verify the ground state configurations, we perform MD simulations at high temperatures. Structural optimization of intermediate configurations from such simulations do not exhibit any tendency to form clusters. There is no evidence of any further splitting of $\mathrm{OH^-} \rightarrow \mathrm{H^+} + \mathrm{O^{2-}}$ and the ratio of hydrogen interstitials attached to oxygen interstitials (in vacant oxygen lattice sites) and hydrogen interstitials in the octahedral voids remains very close to 1:1 for all the analyzed structures. The formation free energy analysis (presented in Fig. 3) on the other hand that shows that $F_\mathrm{f}\left(\mathrm{H^+}\right) + F_\mathrm{f}\left(\mathrm{O^{2-}}\right) \approx F_\mathrm{f}\left(\mathrm{OH^-}\right)$ meaning that $\mathrm{OH^-}$ interstitial can split into $\mathrm{H^+}$ and $\mathrm{O^{2-}}$. Here we note that the magnitude of the periodic image correction for $F_\mathrm{f}\left(\mathrm{O^{2-}}\right)$ is 0.84 eV, and it is plausible that this large correction artificially lowers the formation energy of a O_i^{2-} interstitial. Another possibility is that $F_\mathrm{f}\left(\mathrm{H^+}\right) + F_\mathrm{f}\left(\mathrm{O^{2-}}\right)$ and $F_\mathrm{f}\left(\mathrm{OH^-}\right)$ are indeed close, but their difference is non-zero and our short-MD trajectories are unable to access the time-scales needed to explore the splitting of $\mathrm{OH^-}$.

Defect kinetics: By systematically analyzing the time evolution of $\mathrm{H^+}$ interstitials in vacant oxygen lattice sites and in octahedral voids we see that these defects exhibit a caging behavior, i.e. they are trapped inside the octahedron formed by the six surrounding indium atoms. MD trajectories show that a hydrogen interstitial that is initially bonded to an oxygen hops to another position such that it forms a bond with the oxygen that is next nearest neighbor of its initial position. After some time, this hydrogen hops back to form a bond with its original neighbor. This back and forth movement is also evident from the two-dimensional projection of trajectory of an interstitial hydrogen at 1000 K Fig. $7(a)$. The time evolution of the separation between its current position and its initial position (see Fig. $7(b)$) also shows that this interstitial swaps positions by hopping to different sites but returns to its initial position. These back and forth hopping events are also present in MD simulations performed at 1500 (and at 2000 K) and hydrogen interstitials (in a supercell containing eight water molecules) repeatedly return to form bonds with their original nearest neighbor oxygens. At 2000 K, a few of these interstitials are able to move out of these cages and migrate to positions far away from their initial locations.

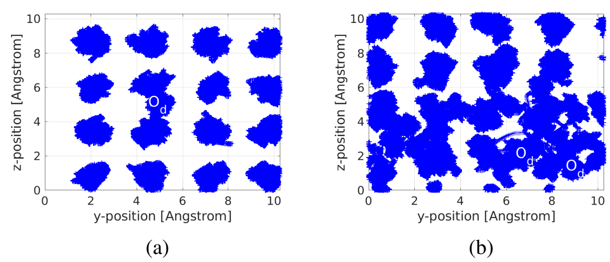

FIG. 6: Shown here are the two-dimensional projections of positions of all oxygens in the supercell for all structures obtained from MD simulations at 1000 K. $6(a)$ shows the local distortion in a supercell containing one water molecule: an oxygen is displaced from its lattice site to the site marked $\mathrm{O_d}$ and forms a bond with a hydrogen interstitial at the octahedral void. $6(b)$ shows the distortion in the oxygen sub-lattice in a supercell containing eight water molecules.

To explore if some of the hydrogen interstitials exist as hydrogen molecules, we analyze the separation between two hydrogens in the different MD trajectories. However, we do not find any $\mathrm{H_2}$ molecules in structures obtained from MD simulations. This is further verified by performing structural relaxations of the configurations obtained from MD simulations. We also probe the ground state structure when two hydrogens are placed close to each other at various different orientations and geometries. However, all such combinations seem to be unstable and the hydrogens move away from each other and form O−H bonds with oxygens present in the system.

Hydrogen bond network: Interestingly, upon incorporating multiple water molecule into the system, we see a very strong evidence of the formation of a hydrogen bond network in the

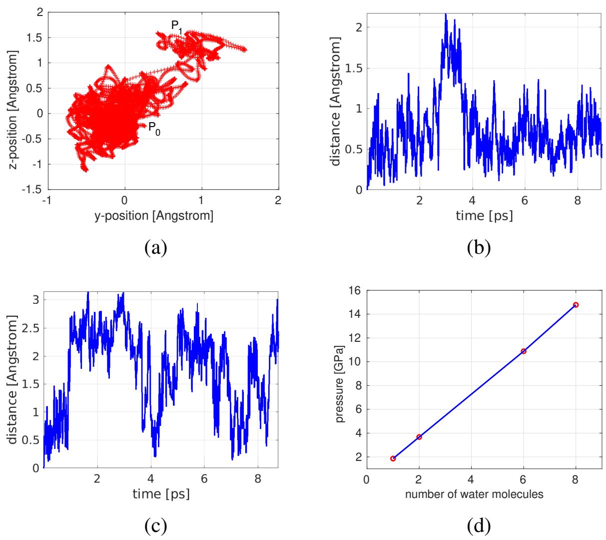

FIG. 7: High temperature MD simulations show that a hydrogen interstitial initially attached to an oxygen hops to a position such that it forms a bond with an oxygen that is the next nearest neighbor of the initial site. $7(a)$ shows the two-dimensional projection of the trajectory of a hydrogen interstitial (one water molecule in a 80 atoms box) at 1000 K and $7(b)$ shows the distance between the initial state and the position at any time. $7(c)$ shows the distance between the initial state and the evolution of the position of the interstitial along a MD trajectory at 1500 K. $7(d)$ shows the pressure, p, on the system as a function of the number of water molecules. The solid line corresponds to the equation $p \approx 1.837 n_{\mathrm{H_2O}} - 0.01$ GPa.

system. One such instance is shown in Fig. 8. In such structures, O−H bond lengths are between 0.96-1.03 Å and distances between hydrogens and next nearest neighbor oxygens are between 1.41-1.90 Å. Similarly, angles between vectors joining hydrogens with their nearest and next nearest neighboring oxygens are between 130-175°. In addition, there are multiple instances, when a transient structure, in which three hydrogens are close to an oxygen is visible: one of these hydrogens forms a O−H bond (mean bond length ∼0.99 Å) and the mean distance between the oxygen and the other two hydrogens is ∼1.60 Å. Even though this transient structure is different from the structure of a hydronium ion, H_3O^+, it is a possible intermediate state during the migration of H^+ or OH^- interstitials. The formation of this hydrogen bond network may also suggest a driving force to local indium hydroxide formation with increased water incorporation. Whether this is occurring and is related to saturation in carrier concentrations in In_2O_3:H with varying water contents needs further investigation.

Possibility of swelling: To analyze if doping by hydrogen can lead to swelling of In_2O_3 films, we calculate the pressure in the system after incorporating water molecules. For these calculations, the supercell volume is same as that of pure In_2O_3. We see that incorporating a water molecule results in a pressure of 1.86 GPa while incorporating eight water molecules results in a pressure of 14.78 GPa. Figure $7(d)$ shows that the pressure on the system increased monotonously with an increase in the number of water molecules and obeys a linear relationship: $p \approx 1.837 n_{\mathrm{H_2O}} - 0.01$ GPa. For the sake of comparison, we note that the pressure when an oxygen (i.e. O^{2-}) or a hydrogen interstitial (i.e. H^+) is present in In_2O_3 is 4.47 and -1.02 GPa, respectively. In contrast, the formation of an oxygen vacancy results in a pressure of -3.89 GPa. Thus, the pressure on the system in presence of water molecules in In_2O_3 is mainly due to the incorporation of oxygens into the system via water. This means that pressure in the bulk regions of an indium oxide film containing hydrogen at 4 at.% concentration (used in experiments) is about 4 GPa.

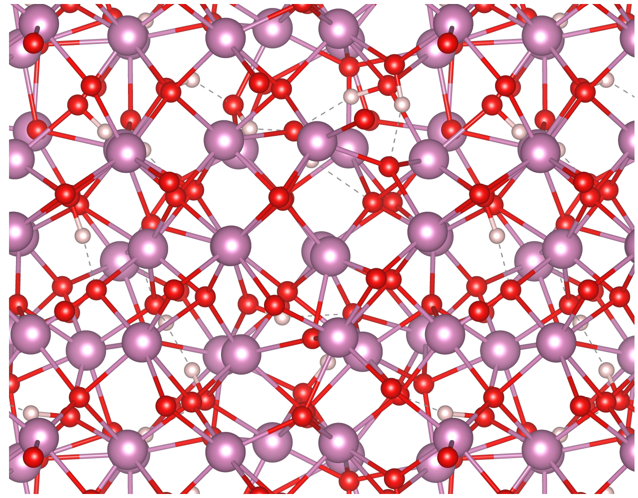

FIG. 8: A snapshot showing the hydrogen bonds (marked using dashed lines connecting a hydrogen with a lattice oxygen) in a supercell containing 8 water molecules (split into H^+ and OH^-). Our results suggest that majority of the OH^- interstitials occupy vacant oxygen lattice sites and the H^+ interstitials occupy the octahedral voids. The presence of H^+ in octahedral voids leads to significant distortion of the oxygen sub-lattice.

IV. CONCLUSIONS

From our analysis of defects in In_2O_3, we reach the following conclusions: (i) Water molecules in In_2O_3 spontaneously splits into H^+ and OH^-. The OH^- interstitial occupies the vacant oxygen lattice sites and eliminates oxygen vacancies already present in a In_2O_3 film. Here we note that one oxygen per formula unit is missing in In_2O_3 compared to the ZrO_2 (i.e. CaF_2 lattice). (ii) The H^+ and OH^- interstitials in In_2O_3 do not form clusters. (iii) Our results show that an oxygen molecule also splits into two oxygen interstitials and these defects occupy the vacant oxygen lattice sites or the octahedral voids. At lower concentration (i.e. at low p_{O_2}), oxygen interstitials energetically prefer vacant oxygen lattice sites. (iv) A hydrogen molecule also splits into two H^+ interstitials. These defects form bonds with oxygens present in In_2O_3 lattice or oxygen interstitials. (v) In case of the OH^- interstitial, the formation free energy is close to the formation energy of a pair of isolated oxygen and hydrogen interstitials. This suggests that during synthesis, OH^- interstitial can spit into an oxygen interstitial and H^+. Thus, In_2O_3 can completely split water molecules into H^+ and O_i^{2-}. (vi) H^+ has lower formation energy than V_O^{2+} when the Fermi level is close to the conduction band. Here we note that if we consider only intrinsic defects, the Fermi level is pinned close to the conduction band at room temperature (or synthesis temperature) and at low oxygen partial pressures. (vii) At high concentrations of incorporated water, these defects form a hydrogen bond network and the oxygen sub-lattice of In_2O_3 is distorted. Such large lattice distortions, when many water molecules are present in In_2O_3, can increase scattering and decrease carrier mobility.

1. *Synthesis in presence of hydrogen and oxygen gas mixture*

Let us focus on the synthesis of In_2O_3:H in the presence of a oxygen and hydrogen gas mixture. In the dilute limit, oxygen interstitials fill up the vacant oxygen lattice sites. This means that up to 16 oxygen interstitials can be incorporated in the conventional unit cell of In_2O_3 (16 formula units, 80 atoms). The reactions that govern the concentration of anionic defects are:[34–36]

$$\mathrm{O_O} \Longleftrightarrow \mathrm{O_i^{2-}} + \mathrm{V_O^{2+}}, \qquad K_\mathrm{F} = \frac{\left[\mathrm{O_i^{2-}}\right]\left[\mathrm{V_O^{2+}}\right]}{N_\mathrm{a}^2}, \tag{6}$$

$$\mathrm{O_O} \Longleftrightarrow \frac{1}{2}\mathrm{O_2}\,(\mathrm{gas}) + \mathrm{V_O^{2+}} + 2e^-, \quad K_1 = \frac{\left[\mathrm{V_O^{2+}}\right]\left[\mathrm{e^-}\right]^2}{N_\mathrm{a} N_\mathrm{c}^2} p_{\mathrm{O_2}}^{1/2}, \tag{7}$$

$$\mathrm{Null} \Longleftrightarrow \mathrm{e^-} + \mathrm{h^+}, \qquad K_\mathrm{i} = \frac{\left[\mathrm{h^+}\right]\left[\mathrm{e^-}\right]}{N_\mathrm{v} N_\mathrm{c}} = e^{-E_\mathrm{g}/k_\mathrm{B}T}, \tag{8}$$

$$\frac{1}{2}\mathrm{O_2}\,(\mathrm{gas}) \Longleftrightarrow \mathrm{O_i^{2-}} + 2\mathrm{h^+}, \qquad K_2 = \frac{\left[\mathrm{h^+}\right]^2\left[\mathrm{O_i^{2-}}\right]}{N_\mathrm{v}^2 N_\mathrm{a} p_{\mathrm{O_2}}^{1/2}}, \tag{9}$$

$$2\left[\mathrm{O_i}\right]^{2-} + \left[\mathrm{e^-}\right] = 2\left[\mathrm{V_O}\right]^{2+} + \left[\mathrm{h^+}\right]. \tag{10}$$

Here, $[\mathrm{e^-}]$ and $[\mathrm{h^+}]$ are the electron and hole concentrations, respectively, $\left[\mathrm{O_i^{2-}}\right]$ and $\left[\mathrm{V_O^{2+}}\right]$ is the oxygen interstitial and vacancy concentration, respectively, N_a is the concentration of anionic sites and E_g is the band gap. The constants N_c and N_v ($N_\mathrm{c} = 2\left(2\pi m_\mathrm{e}^* k_\mathrm{B} T/h^2\right)^{3/2}$ and $N_\mathrm{v} = 2\left(2\pi m_\mathrm{h}^* k_\mathrm{B} T/h^2\right)^{3/2}$) are used to normalize the electron and hole concentration.

Since a hydrogen gas molecule splits into H^+ interstitials, we also need to consider the following reaction

$$\frac{1}{2}\mathrm{H_2}\,(\mathrm{gas}) \Longleftrightarrow \mathrm{H^+} + \mathrm{e^-}, \qquad K_\mathrm{H} = \frac{\left[\mathrm{H^+}\right]\left[\mathrm{e^-}\right]}{N_\mathrm{a} N_\mathrm{c} p_{\mathrm{H_2}}^{1/2}}. \tag{11}$$

Thus, the charge neutrality condition in Eq. 10 becomes

$$2\left[\mathrm{O_i}\right]^{2-} + \left[\mathrm{e^-}\right] = 2\left[\mathrm{V_O}\right]^{2+} + \left[\mathrm{H^+}\right] + \left[\mathrm{h^+}\right]. \tag{12}$$

But, in the oxygen rich environment used for the synthesis of In_2O_3, the effect of oxygen vacancies can be neglected. Thus, Eq. 12 simplifies to

$$2\left[\mathrm{O_i}\right]^{2-} + \left[\mathrm{e^-}\right] = \left[\mathrm{H^+}\right] + \left[\mathrm{h^+}\right]. \tag{13}$$

When the Fermi level is close to the conduction band minimum, from Fig. 3 we see that the formation energy of oxygen vacancies and interstitials are higher than hydrogen interstitials. Thus, in line with the Brouwer approximation, at intermediate pressures the charge neutrality condition in Eq. 13 can be further simplified to $[\mathrm{e^-}] \approx [\mathrm{H^+}]$ meaning that from Eq. 11 we get $[\mathrm{H^+}] = [\mathrm{e^-}] \propto p_{\mathrm{H_2}}^{1/4}$

2. *Synthesis in presence of water vapor*

When hydrogen-doped In_2O_3 films are synthesized in the presence of water vapor, the important reaction is

$$\mathrm{H_2O}\,(\mathrm{gas}) \Longleftrightarrow \mathrm{H^+} + \mathrm{OH^-}, \qquad K_\mathrm{w} = \frac{\left[\mathrm{H_i^+}\right]\left[\mathrm{OH_i^-}\right]}{p_{\mathrm{H_2O}}}. \tag{14}$$

From Fig. 3, we see that when Fermi level is close to the valence band, the formation energy of H^+ is much lower than the formation energy of a OH^- interstitial. However, when the Fermi level is close to the conduction band, the formation energies of these interstitial defects are very close. Thus, when the Fermi level is close to the conduction band, we have $\left[\mathrm{H_i^+}\right] \approx \left[\mathrm{OH_i^-}\right]$ and from Eq. 14 we obtain $\left[\mathrm{H_i^+}\right] \approx \left[\mathrm{OH_i^-}\right] \approx p_{\mathrm{H_2O}}^{1/2}$.

3. *Comparison between water vapor and hydrogen gas synthesis procedures*

From the preceding analyses it is clear that at the same partial pressures of hydrogen gas mixture ($\left[\mathrm{H_i^+}\right] \approx p_{\mathrm{H_2}}^{1/4}$) and water vapor ($\left[\mathrm{H_i^+}\right] \approx p_{\mathrm{H_2O}}^{1/2}$), the concentrations of H^+ interstitials will be different, i.e. the number of hydrogens present in the system is lower when synthesis is performed in presence of hydrogen gas. This is in agreement with the results of SIMS analysis by Jost et al. that showed the hydrogen content of optimal films deposited with hydrogen gas mixture is ∼23% lower than films synthesized using water vapor.[8]

4. Importance and responsivity as a sensor

In_2O_3 is a proposed candidate material for detecting gases like hydrogen. For example, Zheng et al. observed a steady response from sensors made from In_2O_3 nanostructures for up to 30 days.[24] Zheng et al. attributed this sensing property of these one-dimensional In_2O_3 nanostructures of chemisorbed oxygens and abundance of oxygen vacancies. While the characteristic features of the surface of a nano-wire and the interaction of a hydrogen molecule with the surface can differ from the way a hydrogen molecule reacts with bulk In_2O_3, our results suggest that hydrogen molecule splits into H^+ interstitials in bulk In_2O_3:

$$\frac{1}{2}\mathrm{H_2} \rightarrow \mathrm{H^+} + \mathrm{e^-}, \tag{15}$$

and these interstitials form O−H bonds with lattice oxygens. In addition, from the formation free energy analysis it is clear that when oxygen partial pressure is very low compared to the hydrogen partial pressure, the formation energy of a H^+ interstitial is lower than that of an oxygen vacancy. This regime corresponds to the case when the Fermi level is close to the conduction band minimum. Thus, under these conditions, the conductivity of hydrogen-doped indium oxide is governed by $[\mathrm{H^+}] = [\mathrm{e^-}] \propto p_{\mathrm{H_2}}^{1/4}$.

Acknowledgments

This work was performed under the auspices of the U.S. Department of Energy by Lawrence Livermore National Laboratory under Contract DE-AC52-07NA27344. Computing support for this work came from the Lawrence Livermore National Laboratory Institutional Computing facilities. Funding was provided by the Department of Energy office of Energy Efficiency & Renewable Energy (EERE) through the Physics of Reliability: Evaluating Design Insights for Component Technologies in Solar 2 (PREDICTS 2) program. We acknowledge fruitful discussions with M. Bora at Lawrence Livermore National Laboratory.

Data availability The data that support the findings of this study are available from the corresponding author upon reasonable request.

IM release: LLNL-JRNL-812492

---

* Electronic address: samanta1@llnl.gov

1. T. Koida, H. Fujiwara, and M. Kondo, Japanese Journal of Applied Physics **46**, L685 (2007).
2. T. Koida, H. Fujiwara, and M. Kondo, Solar Energy Materials and Solar Cells **93**, 851 (2009).
3. T. Koida, M. Kondo, K. Tsutsumi, A. Sakaguchi, M. Suzuki, and H. Fujiwara, Journal of Applied Physics **107**, 033514 (2010).
4. I. Hamberg and C. G. Granqvist, Journal of Applied Physics **60**, R123 (1986).
5. Y. Shigesato, S. Takaki, and T. Haranoh, Journal of Applied Physics **71**, 3356 (1992).
6. G. B. González, T. O. Mason, J. P. Quintana, O. Warschkow, D. E. Ellis, J.-H. Hwang, J. P. Hodges, and J. D. Jorgensen, Journal of Applied Physics **96**, 3912 (2004).
7. B. Macco, M. A. Verheijen, L. E. Black, B. Barcones, J. Melskens, and W. M. M. Kessels, Journal of Applied Physics **120**, 085314 (2016).
8. G. C. E. Jost, A. N. Hamri, F. Köhler, and J. Hüpkes, Physica Status Solidi A **213**, 1751 (2016).
9. Y. Wu, B. Macco, D. Vanhemel, S. Kölling, M. A. Verheijen, P. M. Koenraad, W. M. M. Kessels, and F. Roozeboom, ACS Applied Materials & Interfaces **9**, 592 (2017).
10. S. Limpijumnong, P. Reunchan, A. Janotti, and C. G. Van de Walle, Physical Review B **80**, 193202 (2009).
11. A. Samanta, J. B. Varley, and V. Lordi, Applied Physics Letters **117**, 62103 (2020).
12. P. D. C. King, T. D. Veal, D. J. Payne, A. Bourlange, R. G. Egdell, and C. F. McConville, Physical Review Letters **101**, 116808 (2008).
13. P. D. C. King, R. L. Lichti, Y. G. Celebi, J. M. Gil, R. C. Vilão, H. V. Alberto, J. Piroto Duarte, D. J. Payne, R. G. Egdell, I. McKenzie, et al., Physical Review B **80**, 081201 (2009).
14. P. Ágoston and K. Albe, Phys. Chem. Chem. Phys. **11**, 3226 (2009).
15. P. Ágoston and K. Albe, Physical Review B **81**, 195205 (2010).
16. P. Reunchan, X. Zhou, S. Limpijumnong, A. Janotti, and C. G. V. de Walle, Current Applied Physics **11**, S296 (2011), ISSN 1567-1739, joint International Conference on the 7th Asian Meeting on Ferroelectricity (AMF-7) and the 7th Asian Meeting on Electroceramics.
17. J. Liu, T. Liu, F. Liu, and H. Li, RSC Advances **4**, 36983 (2014).
18. I. Chatratin, F. P. Sabino, P. Reunchan, S. Limpijumnong, J. B. Varley, C. G. Van de Walle, and A. Janotti, Physical Review Materials **3**, 074604 (2019).
19. J. A. Libera, J. N. Hryn, and J. W. Elam, Chemistry of Materials **23**, 2150 (2011).
20. M. Boccard, N. Rodkey, and Z. C. Holman, Energy Procedia **92**, 297 (2016), ISSN 1876-6102, proceedings of the 6th International Conference on Crystalline Silicon Photovoltaics (SiliconPV 2016).
21. Y. Kuang, B. Macco, B. Karasulu, C. K. Ande, P. C. Bronsveld, M. A. Verheijen, Y. Wu, W. M. Kessels, and R. E. Schropp, Solar Energy Materials and Solar Cells **163**, 43 (2017).
22. S. Li, Z. Shi, Z. Tang, and X. Li, Journal of Alloys and Compounds **705**, 198 (2017).
23. J. Keller, A. Aijaz, F. Gustavsson, T. Kubart, L. Stolt, M. Edoff, and T. Törndahl, Solar Energy Materials and Solar Cells **157**, 757 (2016).
24. Z. Q. Zheng, L. F. Zhu, and B. Wang, Nanoscale Research Letters **10**, 293 (2015).
25. J. Heyd, G. E. Scuseria, and M. Ernzerhof, Journal of Chemical Physics **118**, 8207 (2003).
26. G. Kresse and J. Furthmuller, Physical Review B **54**, 11169 (1996).
27. G. Kresse and J. Furthmuller, Computational Materials Science **6**, 15 (1996).
28. G. Makov and M. C. Payne, Physical Review B **51**, 4014 (1995).
29. P. D. C. King, T. D. Veal, F. Fuchs, C. Y. Wang, D. J. Payne, A. Bourlange, H. Zhang, G. R. Bell, V. Cimalla, O. Ambacher, et al., Physical Review B **79**, 205211 (2009).

[30] R. Ramprasad, H. Zhu, P. Rinke, and M. Scheffler, Physical Review Letters **108**, 066404 (2012).
[31] A. Walsh, J. L. F. Da Silva, S.-H. Wei, C. Körber, A. Klein, L. F. J. Piper, A. DeMasi, K. E. Smith, G. Panaccione, P. Torelli, et al., Physical Review Letters **100**, 167402 (2008).
[32] K. Irmscher, M. Naumann, M. Pietsch, Z. Galazka, R. Uecker, T. Schulz, R. Schewski, M. Albrecht, and R. Fornari, Physica Status Solidi A **211**, 54 (2014).
[33] Y. Kang, G. Kang, H.-H. Nahm, S.-H. Cho, Y. S. Park, and S. Han, Physical Review B **89**, 165130 (2014).
[34] A. Samanta and S. B. Zhang, Applied Physics Letters **101**, 181906 (2012).
[35] A. Samanta, W. E, and S. B. Zhang, Physical Review B **86**, 195107 (2012).
[36] A. Samanta, Journal of Materials Science **51**, 4845 (2016).
[37] J. P. Perdew, K. Burke, and M. Ernzerhof, Physical Review Letters **77**, 3865 (1996).
[38] The magnitudes of corrections due to periodic image interactions for these defects (i.e. supercells containing four or more H^{+}) are quite large (i.e. proportional to 4^2 and 5^2) and they are much larger than the band-gap. Therefore, such corrections are not applied to these defect formation energies.
[39] Here we note that in Fig. $3(a)$, all formation energies except that of two oxygen interstitials are corrected for periodic image interactions. This correction is rather large (about 3.36 eV $> E_{\rm g}$) for a supercell containing two O_i^{2-} interstitials and artificially lowers the corresponding formation energy. Therefore, we have not applied it to supercells containing 3 or more extra electrons.